Recognizing AR-guided manual tasks through autonomic nervous system correlates: a preliminary study

1st Mimma Nardelli
Research Center "E. Piaggio"
University of Pisa
Pisa, Italy
m.nardelli@ing.unipi.it

2nd Sara Condino
Dip. di ingegneria dell'informazione,
EndoCAS Center, University of Pisa
Pisa, Italy
sara.condino@endocas.unipi.it

3rd Shadi Ghiasi
Research Center "E. Piaggio"
University of Pisa
Pisa, Italy
shadi.ghiasi@centropiaggio.unipi.it

4th Alejandro Luis Callara
Research Center "E. Piaggio"
University of Pisa
Pisa, Italy
alejandro.callara@ing.unipi.it

5th Gianluca Rho
Dip. di ingegneria dell'informazione
University of Pisa
Pisa, Italy
gianluca.rho@phd.unipi.it

6th Marina Carbone
EndoCAS Center
University of Pisa
Pisa, Italy
marina.carbone@endocas.org

7th Vincenzo Ferrari
Dip. di ingegneria dell'informazione,
EndoCAS Center, University of Pisa
Pisa, Italy
vincenzo.ferrari@unipi.it

8th Enzo Pasquale Scilingo
Dip. di ingegneria dell'informazione
University of Pisa
Pisa, Italy
enzo.scilingo@unipi.it

9th Alberto Greco
Dip. di ingegneria dell'informazione
University of Pisa
Pisa, Italy
orcid.org/0000-0002-4822-5562

***Abstract*—Optical see-through head-mounted displays (HMD) enable optical superposition of computer-generated virtual data onto the user's natural view of the real environment. This makes them the most suitable candidate to guide manual tasks, as for augmented reality (AR) guided surgery. However, most commercial systems have a single focal plane at around 2-3 m inducing "vergence-accommodation conflict" and "focal rivalry" when used to guide manual tasks. These phenomena can often cause visual fatigue and low performance. In this preliminary study, ten subjects performed a precision manual task in two conditions: with or without using the AR HMD. We demonstrated a significant deterioration of the performance using the AR-guided manual task. Moreover, we investigated the autonomic nervous system response through the analysis of the heart rate variability (HRV) and electrodermal activity (EDA) signals. We developed a pattern recognition system that was able to automatically recognize the two experimental conditions using only EDA and HRV data with an accuracy of 75%. Our learning algorithm highlighted two different physiological patterns combining parasympathetic and sympathetic information.**

***Index Terms*—Head mounted displays (HMDs), optical see-through (OST), vergence-accommodation conflict (VAC), autonomic nervous system (ANS), heart rate variability (HRV), electrodermal activity (EDA), support vector machine (SVM)**

The research leading to these results has received partial funding from the Italian Ministry of Education and Research (MIUR) in the framework of the CrossLab project (Departments of Excellence).

This research has received partial funding from European Union Horizon 2020 Programme under grant agreement n 824153 of the project "POTION-Promoting Social Interaction through Emotional Body Odours".

Corresponding author: Alberto Greco. Email: alberto.greco@unipi.it

I. Introduction

Head mounted displays (HMDs) implementing optical see-through (OST) paradigm are at the leading edge of wearable augmented reality (AR) research [1]–[3]. Surgical training, medical imaging, vision-related research, teleoperation, and virtual prototyping are some of the large number of HMDs application fields.

The great advantage of these AR systems is the possibility of also providing the operator with a natural view of the real world, characterized by its own full resolution. For instance, this integration of virtual and natural views allows the determination of the hand location during the execution of manual tasks. However, recent studies have highlighted several possible perceptual and technological limitations such as device obtrusiveness, low luminance, small field of view, and the perceptual conflict between 2D virtual image on the surface of projection and three-dimensional (3D) real world. Particularly, the current generation of commercial OST-HMDs typically display virtual reality content on a fixed focal plane positioned at around 2 to 3 m apparent distance or more (infinite). Therefore, when such devices are improperly used within the peripersonal space (e.g to guide manual tasks) the virtual content is projected outside the user's eye depth of field leading to two issues: the "focal rivalry" (FR) [4] and the vergence-accommodation conflict (VAC) [5], which hinder the visual comfort.

VAC and FR are major problems in precision manual tasks, e.g., AR guided surgery [6], [7], where VR data must be accurately aligned to the real target. Indeed, several previous studies have already shown the negative effects of FR and VAC conflicts on visual fatigue and fusion failure [8]–[11], showing also a reduction of these effects once focus cue correction has been performed [9]. Moreover, a recent study has demonstrated a significant effect of the perceived visual discomfort and mental workload on the user's performance during the execution of AR guided manual task using the Microsoft HoloLens [5]. User's performance was found to be significantly better during the naked eye tests than during AR-guided tasks. In such previous studies, the effect of VAC has been commonly assessed through questionnaires. These have the great disadvantage to be prone to all common pitfalls of subjective measures. The study of the physiological response to visual discomfort has mostly focused on EEG/ERP and oculomotor response analyses, in the context of passive 3D viewing experience and virtual reality (VR) [12]–[14]. Instead, whether the perceived visual discomfort in the AR tasks and the consequent performance deterioration reflect also on the activity of the autonomic nervous system (ANS) has been only marginally investigated [7], [15], [16]. However, the ANS plays a crucial role in stress, mental fatigue and workload [17], [18], and it would be a very interesting source of information to investigate.

Accordingly, in this preliminary study, we have analyzed two of the most used ANS correlates, such as heart rate variability (HRV) and electrodermal activity (EDA), to measure physiological responses in subjects using OST-HMD during AR-guided precision tasks. Particularly, both statistical and classification analyses have been performed to automatically discriminate between the same manual task executed with or without the Microsoft HoloLens display. In addition, the performance of the manual task executed in both conditions has been evaluated.

II. Materials and Methods

A. Subject recruitment and experimental protocol

Twelve right-handed volunteers (age 25 ± 2.85, 5 males) gave their informed consent to take part to the study, self-reporting no history of clinical cardiovascular and mental diseases. All participants declared to have normal vision acuity or corrected-to-normal visual acuity using contact lenses. Visual acuity was verified for monocular and binocular vision, using the Digital Acuity LogMAR Charts from Chart2020. Two subjects data were discarded due to excessive artifact movements.
The experimental protocol was divided into two sessions:

- AR-guided binocular test to evaluate the effect of the FR and VAC
- Binocular Naked eye test

Each participant was asked to repeat three times each of the above mentioned tests, for a total of six trials for each subject enrolled in the study. Each test session was preceded by a resting-state of two minutes (Figure 1). The order of the two tasks were randomized among the subjects.

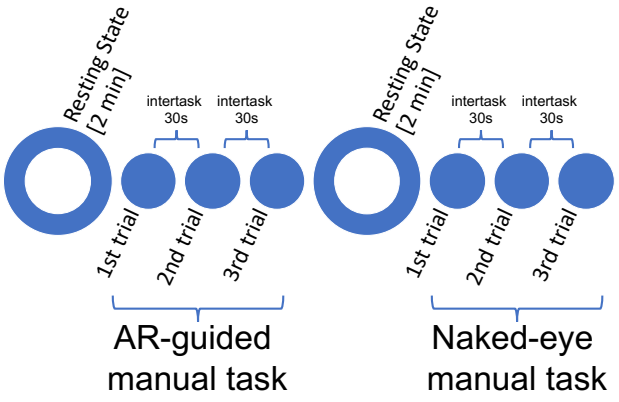

Fig. 1. Exemplary timeline of the experimental protocol.

Fig. 2. Exemplary execution of the AR-guided manual task.

The manual task was designed in order not to require the accurate superimposition of the virtual and physical scenarios. The task consisted of connecting a sequence of numbered dots, drawing lines on a A4 paper positioned on a vertical physical support as shown in Figure 2. A custom Vuforia Image Target (an image with features that Vuforia SDK can detect and track) was used to anchor and display the virtual content at a fixed position in the space as in [2].

During all AR tasks, the numbered dots were projected on a white paper and the subject was asked to draw lines to connect them. During these tasks, the user's eye was forced to be focused on both virtual content (numbered dots) and real objects (pen, ruler, and paper) at the same time. During the naked-eye task, the numbered dots were printed on the

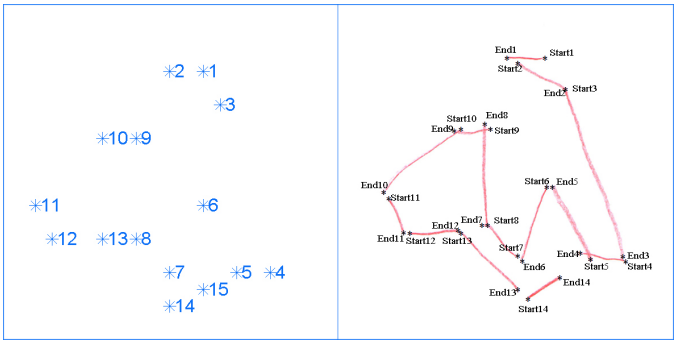

Fig. 3. Example of a task performed with AR. On the left, the virtual content visualized by the subject; on the right, lines drawn by the subject processed to evaluate the performance: the endpoints ($Start_i$, End_i) of each line are represented with black stars.

paper and the subject was asked to draw lines on an overlaying tracing paper.

Considering that the spatial distribution of the numbered dots was changed at each task, a total of six different "connect-the-dots" sequence (CDS) was designed. The difficulty of the tasks was standardized, according to the following criteria:

- connecting lines cannot intersect each-other;
- the distance of two consecutive dots is not fixed, thus connective lines are of different lengths [L1, L2, ... , L14];
- the sequence of distances [L1, L2, . . . , L14] is the same for all the CDS.

Each CDS presented a square area of 15 cm × 15 cm and consists of fifteen dots. Each CDS sequence was randomly associated with each task and the randomization was repeated for each subject.

Before starting the experiment, each participant was asked to calibrate the HoloLens, using the Calibration app (by Microsoft). During the whole experiment, the ECG and the EDA signals were continuously acquired using the BIOPAC MP150 system, which is a 16-Channel data acquisition and analysis system set up at a sampling rate of 500 Hz. Moreover, the EEG signal was recorded using the Geodesic EEG System (EGI), The EEG signal has not been analyzed in this study.

B. Performance evaluation

Each CDS sequence was analyzed to measure subject's performance in connecting dots. Given that eye-to-display calibration errors may lead to a distortion of the perceived virtual content, these can play a major role in the misperception of line lengths. The performance was evaluated in term of gaps (G_{ij}) between the end (End_i) and the starting points ($Start_j$) of each pair (i,j) of consecutive lines. This measure indeed cannot be related to calibration inaccuracies. The line endpoints were automatically detected with the Harris Corner Detector, as described in [5], processing the image drawn by the subject with MATLAB Version R2017b. For each trial the following parameters were calculated: maximum gap (GMAX), mean gap (GMEAN), and total gap (GTOT), i.e. the sum of all the gaps (G_{ij}) measured in the trial.

C. EDA analysis

ECG and EDA dynamics are directly modulated by the ANS activity and, therefore, are considered ideal non-invasive physiological signals to investigate the ANS dynamics. The EDA signal measures the activity of eccrine sweat glands on the hand surface. Since sweat glands are directly innervated by the sympathetic branch of the ANS (and in particular the sudomotor nerve), the EDA analysis is considered one of the best ways to monitor the sympathetic activity. EDA is considered as the superposition of two main components, phasic and tonic, which differ for their time scales and relationships with the external stimuli [19]. In this study, we adopted the well-known cvxEDA model [20] to decompose the EDA signal and extract informative and effective features form both the phasic and tonic signals.

Specifically, EDA algorithm based on Bayesian estimation and convex optimization provides a decomposition of the EDA robust to noise, and enables the estimation of the neural bursts of the sudomotor nerve activity (SMNA), providing a window on the sympathetic nerve activity.

After the application of the cvxEDA model, we extracted several features in order to quantify the activity of the sympathetic nervous system. Particularly, from the SMNA estimated activity signal we calculated the maximum SMNA peak (SMNA_peak) during each trial, the number of the SMNA peaks (SMNA_peak_freq) and the sum of all amplitudes within the trial time window (EDA_AmpSum). From the slow-varying tonic component, we computed the mean and standard deviation within the trial time window (MeanTonic and stdTonic). Finally, we estimated the power spectrum within the frequency range of 0.045 and 0.25Hz (EDAsymp), which has been demonstrated to be strongly correlated to the sympathetic nervous system activity.

D. HRV analysis

From each ECG signal, the interbeat (RR) series was extracted using the Pan-Tompkins algorithm [21]. Artifacts removal was processed through the use of Kubios HRV software [22].

In order to analyze HRV signals related to time windows of the same length, we chose a duration of 25 seconds according to the shortest task execution.

A total amount of eighteen features was extracted from HRV series, in the time and frequency domains, and applying nonlinear analysis in the phase space. In the time-domain, the following four features were calculated for each RR series [23]:

- the mean value of RR intervals (RR mean);
- the standard deviation of RR intervals (RR std);
- the root mean square of successive RR interval differences (RMSSD)
- the relative number of successive RR interval pairs that differ more than 50 msec, expressed as a percentage of the total number of RR intervals (pNN50).

Frequency domain analysis comprised eight features, which were calculated from the Power Spectral Density (PSD) analysis [23]. Two main spectral bands were considered: low frequency (LF) band, ranging between 0.04 and 0.15 Hz, and high frequency (HF) band, comprising frequencies between 0.15 to 0.4 Hz. Then, the following features were computed:

- the power values in LF and HF band (LF power and HF power);
- the power in LF band and HF band normalized to the sum of the LF and HF power (LF nu and HF nu);
- the power in LF band and HF band expressed as percentage of the total power (LF power % and HF power %);
- the ratio between LF power and HF power (LF/HF).

Fuzzy entropy (FuzzyEn) and distribution entropy (DistEn) were used to investigate the irregularity of RR series and the spatial complexity of the related attractors, respectively. Each phase space was reconstructed by setting the time delay and the embedding dimension to $\tau = 1$ and $m = 2$. Starting from a RR series $[rr(i), rr(i+1), ..., rr(N)]$ of N samples, $N - m + 1$ embedded vectors in $\mathbb{R}^m$ were constructed. Each embedding vector $x(i)$ in the phase space was computed as $x(i) = [rr(i), rr(i+1), ..., rr(i+m-1)]$, where i goes from 1 to $N - m + 1$. The Chebyshev distance $d_{i,j}$ between each pair of vectors x_i and x_j was calculated excluding self-matches, and the parameter $F^m(r)$ was calculated as follows:

$$F^m(r) = \frac{1}{N-m} \sum_{i=1}^{N-m} \left(\frac{1}{N-m-1} \sum_{i=1, i \neq j}^{N-m} \Gamma(r - d_{i,j}) \right) \quad (1)$$

where Γ is the function assigning a membership degree to the distances between each pair of vectors, as follows [24]:

$$\Gamma(d_{i,j}, n, r) = e^{-d_{i,j}^{f_p}/r} \quad (2)$$

The power of the fuzzy function f_p was set to 2, in accordance with previous studies [25], [26]. The parameter r is the margin of tolerance used as threshold in the comparison between the vector distances, and in this study was set equal to the 20% of the standard deviation of each series. Increasing the embedding dimension from m to $m + 1$, $F^{m+1}(r)$ was calculated. Finally, the FuzzyEn value was computed as:

$$\text{FuzzyEn(m,r,N)} = -\ln \frac{F^{m+1}}{F^m} \quad (3)$$

DistEn quantifies the complexity of the spatial distribution of the vectors in the phase space [27]–[29]. All the Chebyshev distances d_{ij} among all pairs of embedded vectors in the phase space were found without taking into account the self-matches. Then, the related empirical probability distribution was computed using the histogram approach [27]. The number of bins B was set to 256 [29]. The probability p_b associated to each bin b ($b = 1, ..., B$) was calculated, i.e., $p_b = \frac{\text{count in bin b}}{\text{total elements in D}}$, and DistEn is computed as follows:

$$DistEn(m, B) = -\frac{1}{\log_2(B)} \sum_{t=1}^{B} p_b \log_2(p_b) \quad (4)$$

Furthermore, five features were extracted to quantify the shape of Poincaré map obtained plotting the lagged RR interval series, RR_{n+1}, against the series RR_n. According to the ellipse-fitting technique, the following geometrical parameters were calculated [30], [31]:

- the standard deviation of the points calculated along the direction perpendicular to the line-of-identity $RR_{n+1} = RR_n(SD1)$;
- SD2: the standard deviation of the points along the line-of-identity $RR_{n+1} = RR_n(SD2)$;
- the ratio between SD1 and SD2 (SD12).

Other two Poincaré Plot quantifiers were determined to minimize the loss of information by accounting for the phase space points lying outside the ellipse: namely, the mean (M_d) and the standard deviation (S_d) of the euclidean distances between all the points and the centroid [29].

E. Statistical and classification analysis

Each feature was averaged among the three repetitions of each modality and normalized by subtracting the value computed in the related previous resting session. Wilcoxon non-parametric statistical test was used to compare each feature between the two tasks (i.e., Naked-eye and AR-guided). False discovery rate was controlled through the Benjamini-Yekuteli correction for multiple testing.

Moreover, a dataset with all features was used as the input of a support vector machine (SVM) algorithm to automatically recognize the AR-mediated physiological response from the Naked-eye one. In addition, given the large number of features compared to the small observation, the SVM was combined with a feature selection (FS) strategy based on the Recursive Feature Elimination (RFE) algorithm. The RFE is an embedded FS approach, i.e., it is integrated in the SVM model building the so-called SVM-RFE algorithm. Particularly, RFE is a backward selection strategy, which ranks the features computing an importance score for each feature and recursively removing the least important one. At each RFE iteration, the learning model was validated through a leave-one-subject-out (LOSO) cross-validation strategy, which cyclically trains the model on a set made up of the observations of all the subjects except one and tests it on the remaining subject's data. Results of the sub-feature-set that achieved the most accurate classification will be shown.

III. Results

A. Performance Results

All the subjects did not experience any perceivable jitter/drift of the virtual content, and successfully completed the six tasks. Mean and standard deviation values of GMAX, GMEAN and GTOT are reported in Table I, showing that, on average, subjects performed better during the Naked-eye sessions. The Wilcoxon signed-rank test showed significant

TABLE I
PERFORMANCE EVALUATION RESULTS

Feature	Naked-eye		AR		p-values
	Mean	STD	Mean	STD	
GMAX [mm]	0.2	0.1	0.3	0.1	0.013
GMEAN [mm]	0.1	0.5	0.1	0.1	0.011
GTOT [mm]	0.8	0.5	1.8	0.8	0.004

differences in subject performance depending on the test modalities (p-value$<$0.05).

B. Statistical comparison and Classification Results

The statistical analysis compared each feature of both HRV and EDA between the two tasks. No statistically significant differences were shown considering the single feature individually. However, when mixing EDA and HRV in a multivairate learning model such as the SVM, the classification model was able to automatically discriminate the AR-guided performance from the naked-eye with an average accuracy of 75% (see Figure 4). Moreover, the RFE algorithm selected only three features to reach the maximum accuracy values reducing the risk of overfitting. The features selected were the SD12 of the HRV, the maximum peak of the SMNA response and EDAsymp.

IV. DISCUSSION AND CONCLUSIONS

In this preliminary study, we investigated the ANS response of 10 healthy subjects performing an AR-guided manual task compared to those related to the same task executed without the aid of the AR technology.

We induced participants to use Microsoft HoloLens device wrongly, i.e., without respecting the minimum focal distance, generating the effects known as VAC and FR (i.e., the inability to see simultaneously in focus the virtual and real content). Our study confirmed previous results [5] that these perceptual issues cause a significant worsening of the performance of precision manual tasks when using AR. This bad performance can be associated with a different autonomic physiological response. Indeed, the classification analysis using features extracted from two of the main used ANS correlates such as HRV and EDA, showed good accuracy (i.e., 75%) in distinguishing the manual tasks executed in the two modalities (i.e., with or without the AR help).

Interestingly, the three selected features were extracted from both the EDA and HRV signals. Moreover, while SD12 is considered an index of the parasympathetic activity, both EDAsymp and SMNA_peak measure the activity of the sympathetic nervous system. Therefore, although at speculation level, we can infer that the visual discomfort induced by the AR HMD lead to a different sympathovagal balance in healthy subjects. Note that after a univariate statistical analysis no significant differences were found, instead, combining the feature information into a multivariate learning model two different autonomic patterns have been identified. This is a further confirmation that a multivariate-multiorgan analysis can lead to a better characterization of the ANS dynamics.

This study comes with limitations that make the results just preliminary. Particularly, the low number of subjects performing the study brings the natural consequence of a low statistical power that might hide possible statistical differences. The poor number of observations could also reflect a high risk of overfitting, however the LOSO validation as well as the RFE algorithm, which selected only three features should have mitigated such risk. Moreover, another issue could be related to subjects' degree of pre-learning/familiarity with AR. Indeed, each subject was familiar with the "connecting-the-dots" task in the NK condition, but could not be the same in AR environment.

Future works will strongly increase the number of participants and will combine information coming from the parasympathetic (HRV) and sympathetic (EDA, HRV) nervous systems with those extracted at cortical level thanks to the use of the EEG, in order to build a model that explains the VOC and FR physiological effects. Moreover, possible confounding factors such as the familiarity of the task will be also study

REFERENCES

[1] N. S. Holliman, N. A. Dodgson, G. E. Favalora, and L. Pockett, "Three-dimensional displays: a review and applications analysis," *IEEE transactions on Broadcasting*, vol. 57, no. 2, pp. 362–371, 2011.

[2] J. P. Rolland and O. Cakmakci, "The past, present, and future of head-mounted display designs," in *Optical Design and Testing II*, vol. 5638. International Society for Optics and Photonics, 2005, pp. 368–377.

[3] F. Zhou, H. B.-L. Duh, and M. Billinghurst, "Trends in augmented reality tracking, interaction and display: A review of ten years of ismar," in *2008 7th IEEE/ACM International Symposium on Mixed and Augmented Reality*. IEEE, 2008, pp. 193–202.

[4] K. R. Moser, D. C. Rompapas, J. E. Swan, S. Ikeda, G. Yamamoto, T. Taketomi, C. Sandor, H. Kato *et al.*, "Sharpview: Improved clarity of defocused content on optical see-through head-mounted displays," in *2016 IEEE Symposium on 3D User Interfaces (3DUI)*. IEEE, 2016, pp. 173–181.

[5] S. Condino, M. Carbone, R. Piazza, M. Ferrari, and V. Ferrari, "Perceptual limits of optical see-through visors for augmented reality guidance of manual tasks," *IEEE Transactions on Biomedical Engineering*, 2019.

[6] P. Shao, H. Ding, J. Wang, P. Liu, Q. Ling, J. Chen, J. Xu, S. Zhang, and R. Xu, "Designing a wearable navigation system for image-guided cancer resection surgery," *Annals of biomedical engineering*, vol. 42, no. 11, pp. 2228–2237, 2014.

[7] G. Kramida, "Resolving the vergence-accommodation conflict in head-mounted displays," *IEEE transactions on visualization and computer graphics*, vol. 22, no. 7, pp. 1912–1931, 2015.

[8] J. P. Wann, S. Rushton, and M. Mon-Williams, "Natural problems for stereoscopic depth perception in virtual environments," *Vision research*, vol. 35, no. 19, pp. 2731–2736, 1995.

[9] D. M. Hoffman, A. R. Girshick, K. Akeley, and M. S. Banks, "Vergence–accommodation conflicts hinder visual performance and cause visual fatigue," *Journal of vision*, vol. 8, no. 3, pp. 33–33, 2008.

[10] M. Lambooij, M. Fortuin, I. Heynderickx, and W. IJsselsteijn, "Visual discomfort and visual fatigue of stereoscopic displays: A review," *Journal of Imaging Science and Technology*, vol. 53, no. 3, pp. 30 201–1, 2009.

[11] R. S. Renner, B. M. Velichkovsky, and J. R. Helmert, "The perception of egocentric distances in virtual environments-a review," *ACM Computing Surveys (CSUR)*, vol. 46, no. 2, pp. 1–40, 2013.

[12] S. Mun, M.-C. Park, S. Park, and M. Whang, "Ssvep and erp measurement of cognitive fatigue caused by stereoscopic 3d," *Neuroscience letters*, vol. 525, no. 2, pp. 89–94, 2012.

[13] J. Frey, L. Pommereau, F. Lotte, and M. Hachet, "Assessing the zone of comfort in stereoscopic displays using eeg," in *CHI'14 Extended Abstracts on Human Factors in Computing Systems*, 2014, pp. 2041–2046.

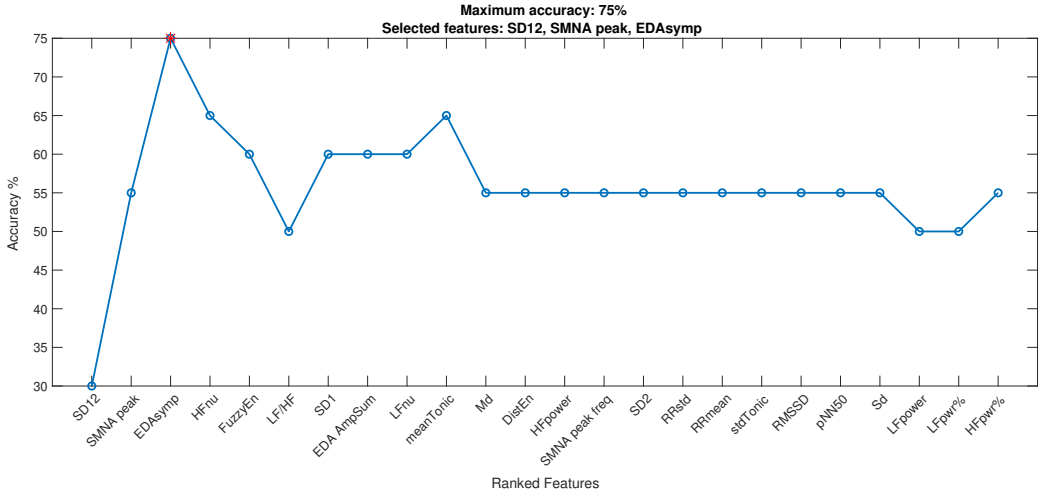

Fig. 4. Classification accuracy

[14] I. Iatsun, M.-C. Larabi, and C. Fernandez-Maloigne, "Investigation of visual fatigue/discomfort generated by s3d video using eye-tracking data," in *Stereoscopic Displays and Applications XXIV*, vol. 8648. International Society for Optics and Photonics, 2013, p. 864803.

[15] H. Oyamada, A. Iijima, A. Tanaka, K. Ukai, H. Toda, N. Sugita, M. Yoshizawa, and T. Bando, "A pilot study on pupillary and cardiovascular changes induced by stereoscopic video movies," *Journal of neuroengineering and rehabilitation*, vol. 4, no. 1, p. 37, 2007.

[16] C. J. Kim, S. Park, M. J. Won, M. Whang, and E. C. Lee, "Autonomic nervous system responses can reveal visual fatigue induced by 3d displays," *Sensors*, vol. 13, no. 10, pp. 13 054–13 062, 2013.

[17] E. Vernet-Maury, C. Deschaumes-Molinaro, G. Delhomme, and A. Dittmar, "Autonomic nervous system activity and mental workload," *International Journal of Psychophysiology*, vol. 14, no. 2, pp. 153–154, 1993.

[18] A. Greco, G. Valenza, A. Bicchi, M. Bianchi, and E. P. Scilingo, "Assessment of muscle fatigue during isometric contraction using autonomic nervous system correlates," *Biomedical Signal Processing and Control*, vol. 51, pp. 42–49, 2019.

[19] A. Greco, G. Valenza, and E. P. Scilingo, *Advances in Electrodermal activity processing with applications for mental health*. Springer, 2016.

[20] A. Greco, G. Valenza, A. Lanata, E. P. Scilingo, and L. Citi, "cvxeda: A convex optimization approach to electrodermal activity processing," *IEEE Transactions on Biomedical Engineering*, vol. 63, no. 4, pp. 797–804, 2015.

[21] J. Pan and W. J. Tompkins, "A real-time qrs detection algorithm," *IEEE transactions on biomedical engineering*, no. 3, pp. 230–236, 1985.

[22] M. P. Tarvainen, J.-P. Niskanen, J. A. Lipponen, P. O. Ranta-Aho, and P. A. Karjalainen, "Kubios hrv–heart rate variability analysis software," *Computer methods and programs in biomedicine*, vol. 113, no. 1, pp. 210–220, 2014.

[23] U. R. Acharya, K. P. Joseph, N. Kannathal, C. M. Lim, and J. S. Suri, "Heart rate variability: a review," *Medical and biological engineering and computing*, vol. 44, no. 12, pp. 1031–1051, 2006.

[24] W. Chen, Z. Wang, H. Xie, and W. Yu, "Characterization of surface emg signal based on fuzzy entropy," *IEEE Transactions on neural systems and rehabilitation engineering*, vol. 15, no. 2, pp. 266–272, 2007.

[25] H. Azami, M. Rostaghi, D. Abásolo, and J. Escudero, "Refined composite multiscale dispersion entropy and its application to biomedical signals," *IEEE Transactions on Biomedical Engineering*, vol. 64, no. 12, pp. 2872–2879, 2017.

[26] M. Nardelli, E. P. Scilingo, and G. Valenza, "Multichannel complexity index (mci) for a multi-organ physiological complexity assessment," *Physica A: Statistical Mechanics and its Applications*, vol. 530, p. 121543, 2019.

[27] P. Li, C. Liu, K. Li, D. Zheng, C. Liu, and Y. Hou, "Assessing the complexity of short-term heartbeat interval series by distribution entropy," *Medical & biological engineering & computing*, vol. 53, no. 1, pp. 77–87, 2015.

[28] C. Karmakar, R. K. Udhayakumar, and M. Palaniswami, "Distribution entropy (disten): a complexity measure to detect arrhythmia from short length rr interval time series," in *2015 37th Annual International Conference of the IEEE Engineering in Medicine and Biology Society (EMBC)*. IEEE, 2015, pp. 5207–5210.

[29] M. Nardelli, A. Greco, O. P. Danzi, C. Perlini, F. Tedeschi, E. P. Scilingo, L. Del Piccolo, and G. Valenza, "Cardiovascular assessment of supportive doctor-patient communication using multi-scale and multi-lag analysis of heartbeat dynamics," *Medical & biological engineering & computing*, vol. 57, no. 1, pp. 123–134, 2019.

[30] M. P. Tulppo, T. Makikallio, T. Takala, T. Seppanen, and H. V. Huikuri, "Quantitative beat-to-beat analysis of heart rate dynamics during exercise," *American journal of physiology-heart and circulatory physiology*, vol. 271, no. 1, pp. H244–H252, 1996.

[31] M. Nardelli, A. Greco, J. Bolea, G. Valenza, E. P. Scilingo, and R. Bailón, "Reliability of lagged poincaré plot parameters in ultrashort heart rate variability series: Application on affective sounds," *IEEE journal of biomedical and health informatics*, vol. 22, no. 3, pp. 741–749, 2017.